Control of Intramolecular Electron Transport Pathways by Varying Localized Electron Distribution

Dahai Zhou
Xiamen University
Ping Duan
Xiamen University
Yu Zhou
Xiamen University
Chuan Li
Chinese Academy of Sciences
Yaping Wang
Xiamen University https://orcid.org/0000-0002-3308-4728
Lichuan Chen
Xiamen University
Jin-Yun Wang
Fujian Institute of Research on the Structure of Matter, Chinese Academy of Sciences
Kai Qu
Chinese Academy of Sciences
Chun Tang
Xiamen University
Jia Shi
Xiamen University
Junyang Liu
Xiamen University
Qian-Chong Zhang
State Key Laboratory of Structural Chemistry, Fujian Institute of Research on the Structure of Matter, Chinese Academy of Science
Zhong-Ning Chen
Fujian Institute of Research on the Structure of Matter, Chinese Academy of Sciences
Wenjing Hong (whong@xmu.edu.cn)
Xiamen University https://orcid.org/0000-0003-4080-6175

Article

Keywords: quantum interference (QI), electron transport pathways, electron distribution

Posted Date: June 17th, 2021

DOI: https://doi.org/10.21203/rs.3.rs-593790/v1

Control of Intramolecular Electron Transport Pathways by Varying Localized Electron Distribution

Dahai Zhou[1†], Ping Duan[1†], Yu Zhou[1†], Chuan Li[2,3,4†], Yaping Wang[1], Lichuan Chen[1], Jin-Yun Wang[2,4], Kai Qu[2,3,4], Chun Tang[1], Jia Shi[1], Junyang Liu[1,*], Qian-Chong Zhang[2,*], Zhong-Ning Chen[2,4,*], and Wenjing Hong[1,*]

[1]State Key Laboratory of Physical Chemistry of Solid Surfaces, *i*ChEM, College of Chemistry and Chemical Engineering, Xiamen University, Xiamen 361005, China

[2]State Key Laboratory of Structural Chemistry, Fujian Institute of Research on the Structure of Matter, Chinese Academy of Sciences, Fuzhou, Fujian 350002, China

[3]School of Physical Science and Technology, ShanghaiTech University, Shanghai 201210, China

[4]University of Chinese Academy of Sciences, Beijing 100049, China

[†]These authors contributed equally.

[*]E-mail: jyliu@xmu.edu.cn; zhangqianchong@fjirsm.ac.cn; czn@fjirsm.ac.cn; whong@xmu.edu.cn

Abstract

The control of different electron transport pathways by quantum interference (QI) effects offers a unique opportunity for the modulation of electrical properties in molecular electronic devices and materials. In this work, we propose a chemical way to control the intramolecular electron transport pathways by the localization of the highest occupied molecular orbital (HOMO) distribution. The negative charge injection in *para*-carbazole by deprotonation exhibited a fourfold suppression of single-molecule conductance, while the conductance is almost the same for *meta*-carbazole before and after deprotonation. The flicker noise analyses and theoretical simulations revealed the localized distribution of HOMO on the *para*-carbazole center, leading to the appearance of destructive quantum interference (DQI) effect for the control of electron transport pathway. This strategy of reaction-induced orbital localization offers a new strategy for the control of charge transport through molecular devices and materials.

Introduction

The electron transport through single-molecule junctions represents the overall contributions of all transport pathways.[1-4] In different electron transport pathways, the phase of transmission amplitudes is different, resulting in different quantum interference (QI) patterns to form various conductance states.[5-8] The QI effects can be regulated through structural modification, such as connection site variation[9-11] and side group substitution,[12-15] which offers the opportunity for the control of specific pathways. However, because of the strong coupling between the molecular energy level and the

Fermi energy level of electrodes, the frontier orbital levels of the molecule are typically overextended, thus inhibiting the formation of destructive quantum interference (DQI).[16, 17] To demonstrate an anti-resonance feature from the DQI for the suppression of charge transport,[18] the localization of electron density distribution of frontier orbitals will be a potential option to avoid this strong coupling.

To reduce the electrode-molecule coupling, the localized distribution can be achieved by chemical design *via* creating the absence of electron density cloud on the connection sites of frontier molecular orbitals.[19] Recent works suggest that the electrode can be decoupled by localizing the lowest unoccupied molecular orbital (LUMO) distribution to form effective DQI to create highly nonlinear I-V features,[19] and also to form the electron-hopping pathway responsible for voltage-induced switching.[20] However, it remains challenging to directly switch between localization and delocalization in single-molecule junctions, the chemical reactions to modify the molecular structure *in-situ* hold a promising way. The chemical reactions, such as isomerization,[21] acidification,[22] photothermal reaction,[23] and redox reaction,[24] provide potentials to change the structure of the molecule and the distribution of electron density cloud. Therefore, regulating the distribution of molecular orbitals through *in-situ* chemical reactions provides a new strategy for controlling the electron transport pathways.

Herein, we synthesized two series of molecules based on carbazole as the conductive core (Figure **1a**), and investigated their single-molecule conductance by the scanning tunneling microscope break junction (STM-BJ) technique.[25, 26] We found that the negative charge injection in *para*-carbazole by deprotonation exhibited a fourfold suppression of single-molecule conductance, while the conductance is almost the same for *meta*-carbazole before and after deprotonation. Further flicker noise measurements and the theoretical simulations, including density functional theory (DFT) combined with non-equilibrium Green's function (NEGF) and electron transport pathway calculations, demonstrated that the localized distribution of HOMO on the *para*-carbazole center leads to the appearance of DQI effect and the control of intramolecular electron transport pathways.

Results

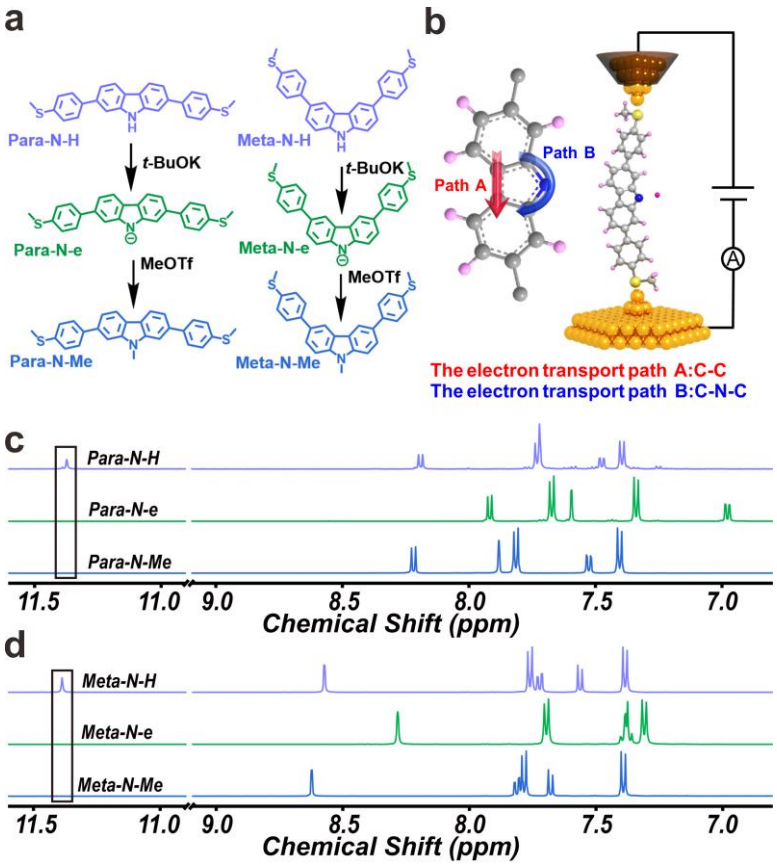

Figure 1 | Molecular structure and ^{1}H NMR of *para*-carbazole and *meta*-carbazole. a, Molecular structure and reaction process of carbazole derivatives. **b**, Schematic of the single-molecule junction, the hafnium dioxide dielectric layer was coated on the gold tip, and the inset indicates two electrical transport pathways in the carbazole ring, C-C and C-N-C. **c**, Monitoring the complete transformation from **Para-N-H** to **Para-N-Me** through ^{1}H NMR. **d**, Monitoring the complete transformation from **Meta-N-H** to **Meta-N-Me** through ^{1}H NMR.

The carbazole compounds are a class of diphenylamine molecules with an isoelectronic structure, which possesses strong electron-donating and hole transport abilities.[27] The proton on the nitrogen atom can be removed through alkalization to create a localized electron density distribution on the carbazole center, and then recovers by acidification,[28] which acts as an ideal platform for regulating electron transport pathways through an *in-situ* chemical reaction.[29, 30] In addition, to quench the negative charge, methyl trifluoromethanesulfonate (MeOTf) was also used to methylate the carbazole anion derivatives to confirm the formation of the localization further.[31] Compound **Para-N-H** and **Meta-N-H** were prepared through the reported procedures (more details in supporting information (SI) section 1).[32, 33] To accurately achieve the

deprotonation of the carbazole structure, potassium *tert*-butoxide (*t*-BuOK) was used as the base to remove the active hydrogen on the nitrogen atom of carbazole, forming a nitrogen anion, which is an extremely hydrogen affinity state. The NMR spectra show that the active hydrogen signal at 11.3 ppm disappears with the addition of base (indicated by the black frame in Figure **1c** and **1d**), while the chemical shifts of other hydrogens move to high-field, which proves the accomplishment of deprotonation.[34, 35] Afterwards, the negative charge can be quenched by methylation with chemical shifts of other hydrogen returning to their original positions and the signal vanishing at 11.3 ppm meanwhile, suggesting the completion of quenching. Single-molecule conductance measurements were conducted for the *para*-carbazole and *meta*-carbazole by using the STM-BJ technique in the solution of N,N-dimethylformamide (DMF) containing 0.1 mM target molecules at the ambient temperatures.

In the investigation of these two states using single-molecule conductance measurement, once high polar DMF as the solvent and a strong base of *t*-BuOK were used, rendering a strong leakage current in this solution environment between the bare Au tip and the Au substrate. It results in a high electrical background and makes conductance testing impossible (more details in Figure S15a and S15b from SI). Therefore, to realize conductance measurement in such an ionic solution system with high polarity and large tunneling background, the tip coated with hafnium dioxide (HfO_2) as the insulating protective layer by Atomic Layer Deposition (ALD) was adopted in the STM-BJ technique.[36] By depositing HfO_2 with a high dielectric constant on the Au tips, we achieved intensive tip coating to significantly reduce the leakage current[37, 38] and the electrical background, which resulted in a larger conductance testing window (more details in SI section 4.2).

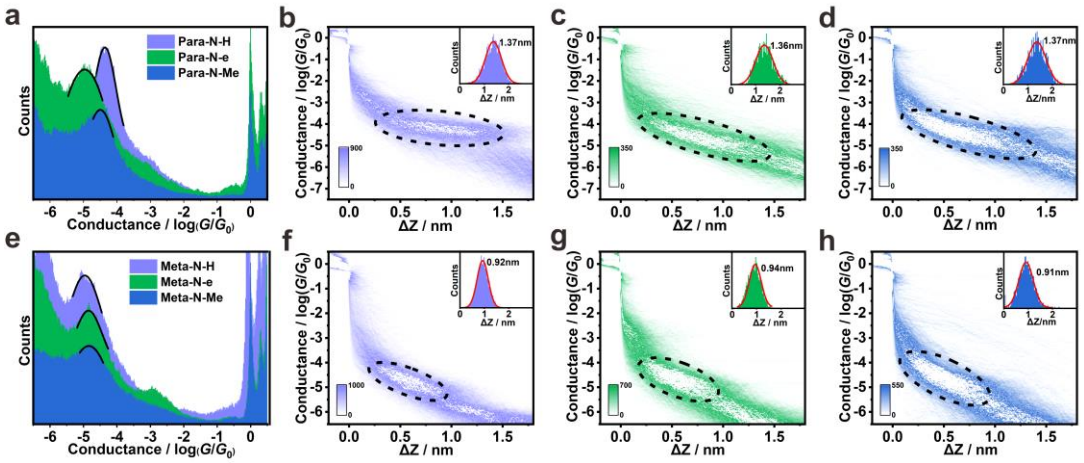

Figure 2 | Conductance measurement results of carbazole derivatives. One-dimensional (1D) conductance histograms of **(a)** *para*-carbazole and **(e)** *meta*-carbazole. Two-dimensional (2D) conductance histograms versus relative displacement and corresponding distributions (inset) of **(b) Para-N-H**, **(c) Para-N-e**, **(d) Para-N-Me**, **(f) Meta-N-H**, **(g) Meta-N-e** and **(h) Meta-N-Me**.

Figure **2a** and **2e** demonstrate the one-dimensional (1D) conductance histogram comparisons of the *para*-carbazole and *meta*-carbazole, respectively, where the peak at G_0 (quantum conductance, $G_0 = 2e^2/h$ = 77.5 μS) illustrates the formation of Au-Au atomic point contact.[39] From the 1D conductance histogram, the single-molecule conductance is determined to be $10^{-4.36}$ G_0 (3.39 nS) for **Para-N-H** and $10^{-4.96}$ G_0 (0.85 nS) for **Meta-N-H**. After the *in-situ* deprotonation by injecting 1 eq. of 1 mM *t*-BuOK, the conductance of deprotonated **Meta-N-e** becomes $10^{-4.85}$ G_0 (1.10 nS), which is slightly higher than that of **Meta-N-H**. However, the conductance of the deprotonated **Para-N-e** decreases to $10^{-4.96}$ G_0 (0.85 nS), which is only a quarter of that of **Para-N-H**. To verify that the significant conductance difference is related to the negative charge on nitrogen atoms, the alkylation reagent of 1.5 mM MeOTf was added to the solution. After alkylation, **Meta-N-Me** and **Meta-N-e** exhibit almost the same conductance, which is $10^{-4.84}$ G_0 (1.12 nS). However, the conductance of **Para-N-Me** is significantly higher than that of **Para-N-e**, which is $10^{-4.49}$ G_0 (2.51 nS) and almost close to that of **Para-N-H**. Therefore, this conductance change must be directly related to the negative charge on nitrogen site. Previous researches have shown that the QI effects can be affected by regulating the charge density of the nitrogen atom on the carbazole ring to change molecular conductance.[40] The charge density of nitrogen atoms can be

characterized by the proton binding ability of nitrogen atoms (*p*Ka). Under acidic and neutral conditions, the molecular conductance increases with the increase of *p*Ka. However, in this experiment, after deprotonation, **Para-N-e** and **Meta-N-e** actually have a strong proton binding ability with large *p*Ka. We found that under alkaline conditions, the conductance of *meta*-carbazole after deprotonation moderately changed, and the regulation effect of *p*Ka reached to saturation, while the conductance of *para*-carbazole after deprotonation decreased, showing an opposite trend compared to previous results.

To seek the origins of the conductance variation, the two-dimensional (2D) conductance and displacement histograms of target molecules are analyzed. The displacement distribution histograms show that the junction lengths of molecules **Para-N-H** (Figure **2b**), **Para-N-e** (Figure **2c**), **Para-N-Me** (Figure **2d**)**, Meta-N-H** (Figure **2f**), **Meta-N-e** (Figure **2g**) and **Meta-N-Me** (Figure **2h**) are 1.37, 1.36, 1.37, 0.92, 0.94 and 0.91 nm, respectively. With the Au-Au snap-back correction of 0.5 nm,[41] the junction lengths of molecules are 1.87, 1.86, 1.87, 1.42, 1.44 and 1.41 nm, respectively, which sufficiently match the S-S distances in the molecules by theoretical calculations (more details in Table S1 from SI), as shown in Table **1**. The junction length correction indicates that the molecular backbone length remains unchanged after deprotonation and alkylation. In addition, we directly synthesized the molecule of **Para-N-Me** and **Meta-N-Me**, by which the test results showed that both the conductance and junction lengths of molecules were consistent with those of the **Para-N-Me** and **Meta-N-Me** formed through *in-situ* alkylation (more details in Figure S16 from SI). Furthermore, to prove the reversibility of this conductance switch, we added an equivalent amount of 1 mM trifluoroacetic acid (TFA) to the solution to neutralize **Para-N-e** into **Para-N-H**, and found that the conductance was reversed. The cycles of protonation and deprotonation can be repeatedly achieved, showing that it is feasible to control the negative charge injection by deprotonation to switch the conductance, as shown in Figure **3a** (more details in Figure S17 from SI). Remarkably, the successive addition of *t*-BuOK and TFA leads to the formation of a large number of ions in the solution, and

experiments show that the HfO_2 coated tip is still suitable for measuring molecular conductance signals in this type of solution with highly concentrated salts.

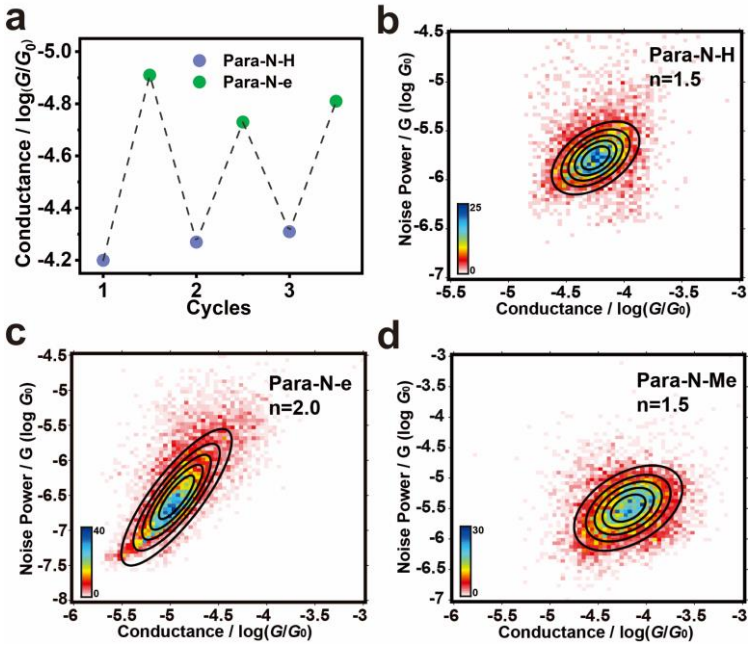

Figure 3 | The conductance cycles measurement and the flicker noise analysis of *para*-carbazole. a, Reversible on-off conductance switching cycles of **Para-N-H** and **Para-N-e** by deprotonation. Two-dimensional histogram of normalized conductance changes versus normalized noise power for **(b) Para-N-H**, **(c) Para-N-e**, **(d) Para-N-Me**.

To further investigate the electrical transport properties before and after deprotonation, the flicker noise measurement was performed. According to the conductance results above, the molecular junction elongation was hovered for 200 ms to extract the conductance signals within the period for flicker noise analysis.[42, 43] We find that the scale of the noise power of **Para-N-H** and **Para-N-Me** is $G^{1.5}$ as shown in Figure **3b** and **3d**, indicating that the charge transport through **Para-N-H** and **Para-N-Me** is synchronously dominated by through-bond and through-space transport. In contrast, for **Para-N-e**, the noise power of $G^{2.0}$ indicates that the through-bond is dominant as shown in Figure **3c**.

The **Para-N-e** and **Meta-N-e** solutions show obvious color changes and different fluorescences before and after deprotonation (more details in Figure S8 from SI). To understand the impact of the injection of negative charge caused by deprotonation on the energy level, we tested the UV-Vis absorption spectra and the fluorescence emission spectra. For **Para-N-e** and **Meta-N-e**, compared with **Para-N-H** and **Meta-N-H**, a new

absorption peak appear at 370 nm and 385 nm (Figure **4a**-**4b)**, respectively, and the emission spectra show obvious redshift (Figure **4d**-**4e**), indicating the shrinkage of energy gaps.[28, 44] After methylation, the UV absorption peaks and the fluorescence emission peaks of **Para-N-Me** and **Meta-N-Me** are basically the same as those of **Para-N-e** and **Meta-N-e**.[45] To further reveal the changes in molecular energy levels before and after deprotonation, density functional theory (DFT) calculations were employed to perform theoretical studies.[46] Frontier molecular orbitals, which are directly correlated to the charge transport, were calculated for all the investigated molecules. Overall, the energy of HOMOs and LUMOs increase with the injection of the negative charge as shown in Figure **4c**. However, the increase of LUMO energy is less than the increase of HOMO energy, which results in narrower HOMO-LUMO gaps. The calculated energy level changes are consistent with the results of macroscopic spectroscopic measurements.

Table 1. Conductance, length and the scale of the noise power from experimental measurements.

Molecule	Measured conductance	Length of molecular junctions / nm	The scale of the noise power
Para-N-H	$10^{-4.36}$ G_0 (3.39 nS)	1.87	1.5
Para-N-e	$10^{-4.96}$ G_0 (0.85 nS)	1.86	2.0
Para-N-Me	$10^{-4.49}$ G_0 (2.51 nS)	1.87	1.5
Meta-N-H	$10^{-4.96}$ G_0 (0.85 nS)	1.42	1.1
Meta-N-e	$10^{-4.85}$ G_0 (1.10 nS)	1.44	1.1
Meta-N-Me	$10^{-4.84}$ G_0 (1.12 nS)	1.41	1.1

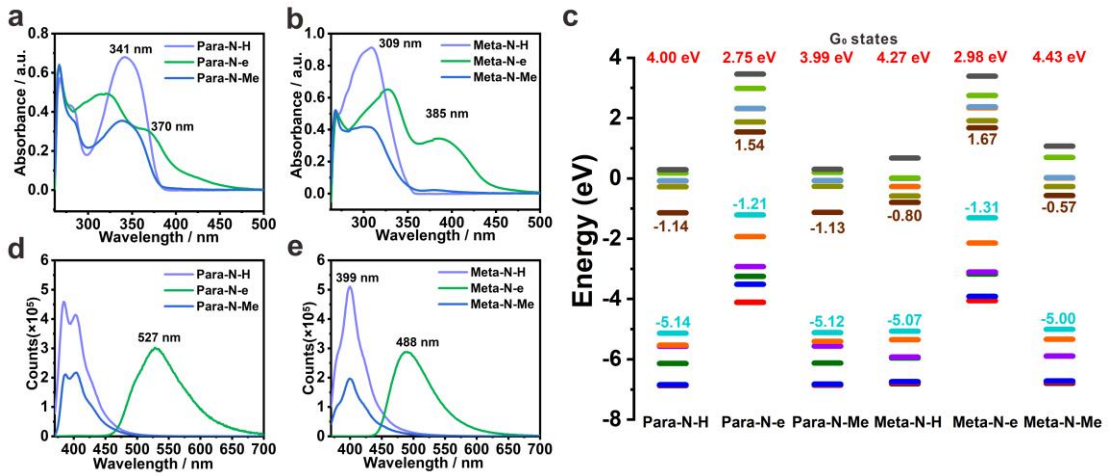

Figure 4 | The spectroscopic characterization and theoretically calculated frontier energy of *para*-carbazole and *meta*-carbazole. UV-Vis absorption spectra of **(a)** *para*-carbazole and **(b)** *meta*-carbazole. **(c)** Theoretically calculated frontier energy and energy gaps between the LUMO and HOMO of *para*-carbazole and *meta*-carbazole. The fluorescence emission spectra of **(d)** *para*-carbazole and **(e)** *meta*-carbazole.

To understand how deprotonation affecting the electron transport in the molecule, the theoretical calculation is employed by the combination of density functional theory (DFT) and non-equilibrium Green's function (NEGF)[47-49] (section 5 in SI). As shown in Figure **5a**, the transmission of **Para-N-e** (green line) is lower than that of **Para-N-H** (purple line) across a wide energy range, which is consistent with the experiments. Meanwhile, the sharp formant between -1 eV and 0 eV, shown in the green curve in Figure **5a**, is the HOMO formant. An obvious dip between the HOMO formant and the LUMO formant indicates that there is a distinct DQI effect between HOMO and LUMO. To further reveal this phenomenon from the perspective of molecular orbital, the spatial distribution of orbital levels of **Para-N-H** and **Para-N-e** are analyzed as shown in Figure **5c**. For **Para-N-H**, HOMO and LUMO orbitals are delocalized. In contrast, for **Para-N-e** formed by deprotonation, the introduction of negative charge causes the localized HOMO and the delocalized LUMO. The localized distribution of electron cloud on HOMO is only on the carbazole fragment, which leads to the weak coupling between HOMO and the electrode Fermi level to some extent. From the Molecular projection self-consistent Hamiltonian (MPSH) states of HOMO for **Para-N-e**, the fact that HOMO is still predominantly distributed on carbazole fragment again indicates a weak coupling between HOMO and the electrode Fermi levels(more details in Figure

S20 from SI). Furthermore, the weak coupling leads to a decrease in the broadening of HOMO formant and a decrease in the resonance energy, resulting in a low and sharp HOMO formant as shown in Figure **5a**. In addition, the localized HOMO and the delocalized LUMO even fulfill the theory of Fano resonance that a localized state interacts with a continuum.[18] In contrast, as shown in Figure **5b**, the transmission of **Meta-N-e** (green line) is slightly higher than that of **Meta-N-H** (purple line) across a wide energy range, which is consistent with the experiments. For **Meta-N-e** formed by deprotonation, the molecular orbitals are closer to the Fermi level than **Meta-N-H**, resulting in a slight increase in conductance. In addition, for **Meta-N-H** and **Meta-N-e**, the electron cloud on the HOMO orbitals is delocalized and not affected by deprotonation, as shown in Figure **5d**. Although the LUMO orbital of **Meta-N-H** seems to be localized, the transmission spectrum of **Meta-N-H** shows that the energy of the LUMO formant is high, which means that the LUMO orbital of the molecule is delocalized, thus without the creation of the DQI effect.

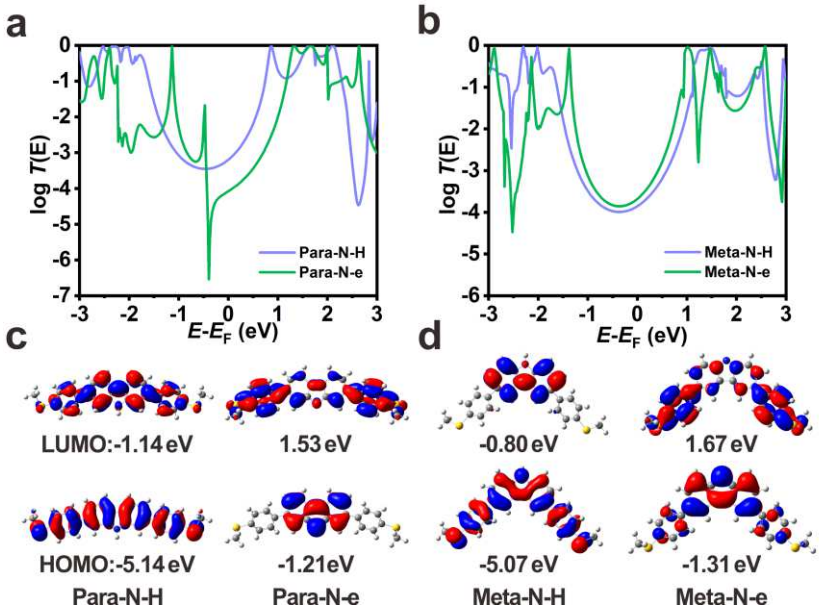

Figure 5 | DFT calculated electrical properties of *para*-carbazole and *meta*-carbazole. Transmission curves of **(a) Para-N-H** (purple line) and **Para-N-e** (green line) and **(b) Meta-N-H** (purple line) and **Meta-N-e** (green line). Spatial distribution of orbital levels of **(c) Para-N-H** (LUMO: -1.14 eV, HOMO: -5.14 eV) and **Para-N-e** (LUMO: 1.53 eV, HOMO: -1.21 eV) and **(d) Meta-N-H** (LUMO: -0.80 eV, HOMO: -5.07 eV) and **Meta-N-e** (LUMO: 1.67 eV, HOMO: -1.31 eV).

To investigate the effect of the introduction of negative charge on the intramolecular electron transport pathway, we calculated the electron transport pathway of **Para-N-H**

and **Para-N-e** as shown in Figure **6a**-**6b** and Table S2 in SI.[50, 51] For **Para-N-H**, electrons are mainly transmitted through the C-C pathway (more details in Table S2, at the energy position of -1.4 eV, the ratio of current in the C-C pathway reached 71.36%), such a *para*-connection pathway does not have DQI effect,[6] thus a higher conductance is revealed, which is also verified on the transmission curve (Figure **5a**, purple line). However, for **Para-N-e**, deprotonation leads to the localization of HOMO orbitals, which further causes the ring current in carbazole center (Figure **6b**). The current direction in carbazole center at different energy positions (-0.5 eV and -0.3 eV) is reversed, which is also a sign of DQI,[52] and the reversed ring current blocks the electron transport pathways of C-C and C-N-C in the molecule, resulting in a significant change of electrical transport properties (more details in Table S2, at the energy of -0.5 eV and -0.3 eV, the current of C-C is capable of that of C-N-C while the direction is opposite). The previous flicker noise measurements also confirmed such changes in intramolecular electron transport pathways. For **Para-N-H**, which mainly transmits electrons through the C-C pathway, its electron transport mode is coupled by both through-bond and through-space, while for **Para-N-e**, due to the DQI effect, the through-bond tunneling is suppressed, thus the through-space tunneling becomes dominant, therefore the noise power changed from 1.5 in **Para-N-H** to 2.0 in **Para-N-e**.[53] On the other hand, for *meta*-carbazole, the electron transport pathways do not significantly change before and after deprotonation, so the electron transport properties remain unchanged. The calculation of transmission pathways shows that electrons in both **Meta-N-H** and **Meta-N-e** are transmitted through the C-N-C pathway as shown in Figure **6c-6d** (more details in Table S2, at the energy position of -1 eV, the ratio of current in the C-N-C pathway for **Meta-N-H** and **Meta-N-e** is 97.77% and 81.90%, respectively). The flicker noise analysis also shows that the noise power of **Meta-N-H** and **Meta-N-e** is $G^{1.1}$ before and after deprotonation, which means that their electrical transport mode remains through-bond tunneling (more details in Figure S19 from SI). The flicker noise remains unchanged before and after deprotonation for *meta*-carbazole, which to some extent proved that the change of flicker noise before and after

deprotonation for *para*-carbazole is due to the change of intramolecular electron transport pathway.

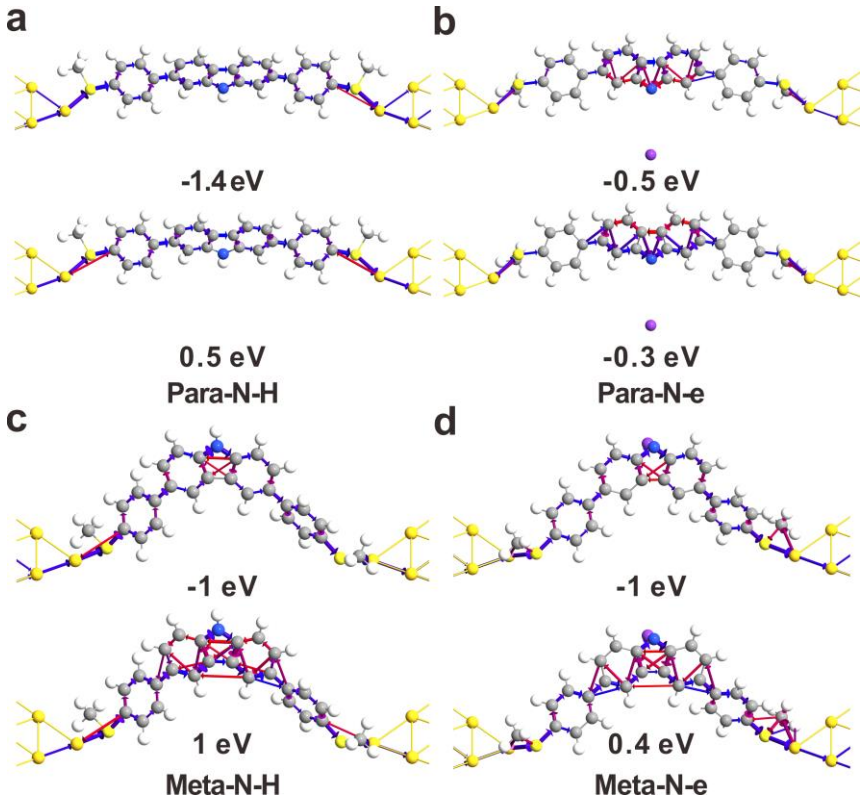

Figure 6 | Transmission pathways of *para*-carbazole and *meta*-carbazole. Transmission pathways of **(a) Para-N-H** at the energy of -1.4 eV (upper panel) and 0.5 eV (lower panel), **(b) Para-N-e** at the energy of -0.5 eV (upper panel) and -0.3 eV (lower panel), **(c) Meta-N-H** at the energy of -1 eV (upper panel) and 1 eV (lower panel) and **(d) Meta-N-e** at the energy of -1 eV (upper panel) and 0.4 eV (lower panel).

Conclusion

In conclusion, the charge transport through single-molecule junctions of *para*-carbazole and *meta*-carbazole before and after deprotonation was investigated using the STM-BJ technique. The results demonstrate that the injection of negative charge *via* the deprotonation of *para*-carbazole leads to a reversible fourfold suppression of conductance. The combined theoretical calculations and the flicker noise analysis revealed that the injection of negative charge results in the localization of HOMO orbitals in *para*-carbazole, leading to the reversed ring current and eventually blocking the intramolecular electrical transport pathways because of DQI. In comparison, the conductance and main electron transport pathway of *meta*-carbazole remain unchanged before and after deprotonation. Our findings provide an *in-situ* strategy for designing

reversible molecular switches to manipulate charge transport through the single-molecule junction, which is achieved *via* blocking the intramolecular transport pathways of electrons by localized electron distribution.

Methods

Materials

The molecules were synthesized according to the previous report (For more details, see supporting information (SI) section 1).[32, 33, 54] For more details, see supporting information (SI) section 1. The gold substrates were prepared by coating 200 nm Au film on silicon wafers. Gold wire (99.99%, 0.25 mm diameter) was purchased from Beijing Jiaming Platinum Nonferrous Metal Co, Ltd. for the fabrication of the gold tip. The hafnium dioxide coated gold tip was prepared by Atomic Layer Deposition (ALD) (For more details, see SI section 4.2).

The STM-BJ measurement

The conductance of molecular junctions was measured using the lab-built scanning tunneling microscope break junction (STM-BJ) technique under ambient conditions (Figure S11).[55, 56] In the STM-BJ measurement, the distance between the gold tip and the substrate is controlled by a stepper motor and a piezo stack. The bias voltage is applied between the tip and substrate, and the current is used as feedback to control the movement of the gold tip. During the repeating opening (tip retracting) and closing (tip approaching) cycles, the conductance versus displacement traces are collected, and the traces of the opening cycles are used for further analysis.

The flicker noise measurement.

The flicker noise measurement carried out according to the previous studies.[42, 52] We suspended the tip during the retracting process for 200 ms after the formation of molecular junctions. The noise spectrums were obtained by the fast Fourier transform. We calculated the noise power according to the noise spectrum integration from 100 Hz to 1000 Hz and plotted the noise power against the average conductance.

Reference

1. Su, T. A., Neupane, M., Steigerwald, M. L., Venkataraman, L. & Nuckolls, C. Chemical principles of single-molecule electronics. *Nat. Rev. Mater.* **1**, 16002 (2016).

2. Huang, C., Rudnev, A. V., Hong, W. & Wandlowski, T. Break junction under electrochemical gating: Testbed for single-molecule electronics. *Chem. Soc. Rev.* **44**, 889-901 (2015).

3. Xin, N. *et al.* Concepts in the design and engineering of single-molecule electronic devices. *Nat. Rev. Phys.* **1**, 211-230 (2019).

4. Komoto, Y., Fujii, S., Iwane, M. & Kiguchi, M. Single-molecule junctions for molecular electronics. *J. Mater. Chem. C.* **4**, 8842-8858 (2016).

5. Liu, J., Huang, X., Wang, F. & Hong, W. Quantum interference effects in charge transport through single-molecule junctions: Detection, manipulation, and application. *Acc. Chem. Res.* **52**, 151-160 (2019).

6. Li, Y. *et al.* Gate controlling of quantum interference and direct observation of anti-resonances in single molecule charge transport. *Nat. Mater.* **18**, 357-363 (2019).

7. Xiang, D., Wang, X., Jia, C., Lee, T. & Guo, X. Molecular-scale electronics: From concept to function. *Chem. Rev.* **116**, 4318-4440 (2016).

8. Lambert, C. J. Basic concepts of quantum interference and electron transport in single-molecule electronics. *Chem. Soc. Rev.* **44**, 875-888 (2015).

9. Xia, J. *et al.* Breakdown of interference rules in azulene, a nonalternant hydrocarbon. *Nano Lett.* **14**, 2941-2945 (2014).

10. Arroyo, C. R. *et al.* Signatures of quantum interference effects on charge transport through a single benzene ring. *Angew. Chem. Int. Ed.* **52**, 3152-3155 (2013).

11. Geng, Y. *et al.* Magic ratios for connectivity-driven electrical conductance of graphene-like molecules. *J. Am. Chem. Soc.* **137**, 4469-4476 (2015).

12. Jiang, F. *et al.* Turning the tap: Conformational control of quantum interference to modulate single-molecule conductance. *Angew. Chem. Int. Ed.* **58**, 18987-18993 (2019).

13. Ismael, A. K. *et al.* Side-group-mediated mechanical conductance switching in molecular junctions. *Angew. Chem. Int. Ed.* **56**, 15378-15382 (2017).

14. Meng, L. *et al.* Side-group chemical gating via reversible optical and electric control in a single molecule transistor. *Nat. Commun.* **10**, 1450 (2019).

15. Soni, S. *et al.* Understanding the role of parallel pathways via in-situ switching of quantum interference in molecular tunneling junctions. *Angew. Chem. Int. Ed.* **59**, 14308-14312 (2020).

16. Guedon, C. M., Valkenier, H., Markussen, T., Thygesen, K. S., Hummelen, J. C. & van der Molen, S. J. Observation of quantum interference in molecular charge transport. *Nat. Nanotechnol.* **7**, 305-309 (2012).

17. Baldea, I., Xie, Z. T. & Frisbie, C. D. Uncovering a law of corresponding states for electron tunneling in molecular junctions. *Nanoscale* **7**, 10465-10471 (2015).

18. Papadopoulos, T. A., Grace, I. M. & Lambert, C. J. Control of electron transport through fano resonances in molecular wires. *Phys. Rev. B* **74**, 193306 (2006).

19. Greenwald, J. E. *et al.* Highly nonlinear transport across single-molecule junctions via destructive quantum interference. *Nat. Nanotechnol.* **16**, 313-317 (2021).

20. Schwarz, F. *et al.* Charge transport and conductance switching of redox-active azulene derivatives. *Angew. Chem. Int. Ed.* **55**, 11781-11786 (2016).

21. Kim, Y. *et al.* Charge transport characteristics of diarylethene photoswitching single-molecule junctions. *Nano Lett.* **12**, 3736-3742 (2012).

22. Yang, G. *et al.* Protonation tuning of quantum interference in azulene-type single-molecule junctions. *Chem. Sci.* **8**, 7505-7509 (2017).

23. Huang, C. *et al.* Single-molecule detection of dihydroazulene photo-thermal reaction using break junction technique. *Nat. Commun.* **8**, 15436 (2017).

24. Chen, F., He, J., Nuckolls, C., Roberts, T., Klare, J. E. & Lindsay, S. A molecular switch based on potential-induced changes of oxidation state. *Nano Lett.* **5**, 503-506 (2005).

25. Xiao, X., Xu, B. & Tao, N. Conductance titration of single-peptide molecules. *J. Am. Chem. Soc.* **126**, 5370-5371 (2004).

26. Haiss, W. *et al.* Precision control of single-molecule electrical junctions. *Nat. Mater.* **5**, 995-1002 (2006).

27. Roy, J., Jana, A. K. & Mal, D. Recent trends in the synthesis of carbazoles: An update. *Tetrahedron* **68**, 6099-6121 (2012).

28. Chattopadhyay, N. Excited state proton transfer of carbazole. A convenient way to study microheterogeneous environments. *Int. J. Mol. Sci.* **4**, 460-480 (2004).

29. Grace, I. M. *et al.* Connectivity dependent thermopower of bridged biphenyl molecules in single-molecule junctions. *Nanoscale* **12**, 14682-14688 (2020).

30. Yamada, R., Albrecht, K., Ohto, T., Minode, K., Yamamoto, K. & Tada, H. Single-molecule rectifiers based on voltage-dependent deformation of molecular orbitals in carbazole oligomers. *Nanoscale* **10**, 19818-19824 (2018).

31. Du, Y., Wu, H., Song, H., Qin, Y. & Zhang, D. Alternative methylation for the synthesis of (+)-perophoramidine. *Chin. J. Chem* . **30**, 1970-1973 (2012).

32. Pascanu, V. *et al.* Sustainable catalysis: Rational pd loading on mil-101cr-nh2 for more efficient and recyclable suzuki-miyaura reactions. *Chem. Eur. J.* **19**, 17483-17493 (2013).

33. Bzeih, T. *et al.* A general synthesis of arylindoles and (1-arylvinyl)carbazoles via a one-pot reaction from n-tosylhydrazones and 2-nitro-haloarenes and their potential application to colon cancer. *Chem. Commun.* **52**, 13027-13030 (2016).

34. Kupka, T., Pasterna, G., Jaworska, M., Karali, A. & Dais, P. Giao nmr calculations for carbazole and its n-methyl and n-ethyl derivatives. Comparison of theoretical and experimental 13c chemical shifts. *Magn. Reson. Chem.* **38**, 149-155 (2000).

35. Bonesi, S. M., Ponce, M. A. & Erra-Balsells, R. A study of substituent effect on 1h and 13c nmr spectra of n- and c-substituted carbazoles. *J. Heterocycl. Chem.* **41**, 161-171 (2004).

36. George, S. M. Atomic layer deposition: An overview. *Chem. Rev.* **110**, 111-131 (2010).

37. Huang, Y. P. *et al.* Shell-isolated tip-enhanced raman and fluorescence spectroscopy. *Angew. Chem. Int. Ed.* **57**, 7523-7527 (2018).

38. Choi, J. H., Mao, Y. & Chang, J. P. Development of hafnium based high-k materials-a review. *Mater. Sci. Eng. R Rep.* **72**, 97-136 (2011).

39. Wu, S. *et al.* Molecular junctions based on aromatic coupling. *Nat. Nanotechnol.* **3**, 569-574 (2008).

40. Naghibi, S. *et al.* Synthetic control of quantum interference by regulating charge on a single atom in heteroaromatic molecular junctions. *J. Phys. Chem. Lett.* **10**, 6419-6424 (2019).

41. Cai, S. *et al.* Light-driven reversible intermolecular proton transfer at single-molecule junctions. *Angew. Chem. Int. Ed.* **58**, 3829-3833 (2019).

42. Adak, O. *et al.* Flicker noise as a probe of electronic interaction at metal-single molecule interfaces. *Nano Lett.* **15**, 4143-4149 (2015).

43. Fu, T. *et al.* Enhanced coupling through pi-stacking in imidazole-based molecular junctions. *Chem. Sci.* **10**, 9998-10002 (2019).

44. Sarkar, D., Mahata, A., Das, P., Girigoswami, A. & Chattopadhyay, N. Excited state proton transfer promoted fluorescence resonance energy transfer: Modulation within cyclodextrin nanocavity. *Chem. Phys. Lett.* **474**, 88-92 (2009).

45. Romero-Ale, E. E., Olives, A. I., Martin, M. A., del Castillo, B., Lopez-Alvarado, P. & Menendez, J. C. Environmental effects on the fluorescence behaviour of carbazole derivatization reagents. *Luminescence* **20**, 162-169 (2005).

46. Tian, G. J. & Luo, Y. Fluorescence and phosphorescence of single c60 molecules as stimulated by a scanning tunneling microscope. *Angew. Chem. Int. Ed.* **52**, 4814-4817 (2013).

47. Soler, J. M. The siesta method for ab initio order-n materials simulation. *J. Phys. Condens. Matter* **14**, 2745-2779 (2002).

48. An, Y. *et al.* Negative differential resistance and rectification effects in step-like graphene nanoribbons. *Org. Electron.* **17**, 262-269 (2015).

49. Kotiuga, M., Darancet, P., Arroyo, C. R., Venkataraman, L. & Neaton, J. B. Adsorption-induced solvent-based electrostatic gating of charge transport through molecular junctions. *Nano Lett.* **15**, 4498-4503 (2015).

50. Li, H. *et al.* Large variations in the single-molecule conductance of cyclic and bicyclic silanes. *J. Am. Chem. Soc.* **140**, 15080-15088 (2018).

51. Hansen, T. & Solomon, G. C. When conductance is less than the sum of its parts: Exploring interference in multiconnected molecules. *J. Phys. Chem. C* **120**, 6295-6301 (2016).

52. Garner, M. H. *et al.* Comprehensive suppression of single-molecule conductance using destructive sigma-interference. *Nature* **558**, 415-419 (2018).

53. Chen, Z. *et al.* Control of quantum interference in single-molecule junctions via jahn-teller distortion. *Cell Rep. Phys. Sci.* **2**, 100329 (2021).

54. Diep, V., Dannenberg, J. J. & Franck, R. W. An o-iminothioquinone: Its cycloaddition to produce an indologlycoside and its self-dimerization to form a dithio-diazocycloctane, the structure assignment of which is based on the dft prediction of its ir spectrum. *J. Org. Chem.* **68**, 7907-7910 (2003).

55. Xu, B. Q. & Tao, N. J. Measurement of single-molecule resistance by repeated formation of molecular junctions. *Science* **301**, 1221-1223 (2003).

56. Tang, C. *et al.* Multicenter-bond-based quantum interference in charge transport through single-molecule carborane junctions. *Angew. Chem., Int. Ed.* **58**, 10601-10605 (2019).

Acknowledgments

We are grateful for financial support from the National Key Research and Development Program of China (2017YFA0204902), the National Natural Science Foundation of China (Nos. 21933012, 31871877, 21601182, 92061117), the Fundamental Research Funds for the Central Universities (20720200068, 20720190002) and the Strategic Priority Research Program of the Chinese Academy of Sciences (Grant XDB20000000).

Author contributions

J. L., W. H. and Z. N. C. co-supervised the project. J. L., D. Z., P. D., Y. Z. and Q. C. Z wrote the manuscript with output from all authors. P. D., C. L. and K. Q. synthesized and provided the structural characterization of the molecules in Z. N. C.'s lab. D. Z., Y. W. and C. T. carried out the break junction experiments and analyzed the data, J. S. and W. H. built the electrical measurement instrument and wrote the software to control the break junction setup, Y. Z., P. D., L. C. and J. Y. W. performed the theoretical modeling in W. H.'s Lab.

Competing interests

The authors declare no competing interests.

Materials & Correspondence

Correspondence and requests for materials should be addressed to Wenjing Hong (whong@xmu.edu.cn).

Supplementary Files

This is a list of supplementary files associated with this preprint. Click to download.

- CarbazolencSupportingInformation20210605.docx